Vilniaus universiteto

Fizikos fakulteto

Taikomosios elektrodinamikos ir telekomunikacijų institutas

Naglis Burdaitis

YSZ keramikų gamybos metodo įtaka jų elektrinėms savybėms

Bakalauro studijų baigiamasis darbas

Šviesos technologijų studijų programa

Studentas	Naglis Burdaitis
Leista ginti	2024-01-10
Darbo vadovas	Prof. Tomas Šalkus
Taikomosios elektrodinamikos ir telekomunikacijų instituto direktorius	Prof. Robertas Grigalaitis

Vilnius 2024

VILNIUS UNIVERSITY
FACULTY OF PHYSICS
INSTITUTE OF APPLIED ELECTRODYNAMICS AND TELECOMMUNICATIONS

Naglis Burdaitis

The Influence of YSZ Ceramics Processing Method on Their Electrical Properties

Bachelor thesis

Light Engineering study programme

Student	Naglis Burdaitis
Approved for defense	10/01/2024
Supervisor	Assoc. prof. Tomas Šalkus
Director of Institute of Applied Electrodynamics and Telecommunications	Prof. Robertas Grigalaitis

Vilnius 2024

Contents

Introduction

The yttria-stabilized zirconia (YSZ) in a ceramic form exhibits excellent electrical properties, high ionic conductivity, thermal stability, and mechanical strength. YSZ is composed of ZrO_2 with added small amounts of Y_2O_3 as a stabilizing agent.

YSZ is a solid electrolyte, and its electrical properties are attributed to the presence of oxygen vacancies in its crystal lattice. High ionic conductivity at elevated temperatures makes it an excellent candidate for solid oxide fuel cells (SOFCs), it enables efficient oxygen ion transport within SOFCs making conversion of chemical energy to electrical energy at high efficiency possible[1]. Reducing the operational temperature of SOFCs is a major concern for SOFCs wider adoption to our energy systems. For this reason, research of new electrolytes with better conductivity at lower temperatures is still ongoing [2]. YSZ is also used for oxygen gas sensors that could help to monitor exhaust gasses of combustion engines[3], separation membranes, oxygen pumps [4]. YSZ has been used in solid oxide electrolysis cells where it helps to more efficiently split water molecules to hydrogen and oxygen using electrical energy[5], [6].

The YSZ is usually made in polycrystalline or ceramic form. Conductivity of ceramics are affected by 1) chemical composition, 2) microstructure. The microstructure of ceramic depends on the sintering technique used. Most common conventional method consists of heating sample in a furnace at sintering temperatures for 1-10 hours, though new novel ways of sintering ceramics show excellent results such as spark plasma sintering (SPS) [7][8], hot pressing [9].

Impedance spectroscopy is a powerful tool used to analyze polycrystalline structures, which allows us to separate different components influence on total samples' conductivity, in this case grain (bulk) conductivity from grain boundary conductivity.

The YSZ ceramics are not a new material, but there are only a few systematic research papers published, especially there is a lack of knowledge about SPS method produced YSZ electrical properties, effects of reduction during SPS compared to conventional method.

The objective of this work is to investigate the influence of sintering temperature, method, size of powder grains on electrical properties of YSZ ceramics using impedance spectroscopy.

1. Literature overview

1.1 YSZ structure

A pure zirconium oxide ZrO_2 forms monoclinic (m) structure at room temperature and atmospheric pressure, at increased temperatures above 1170 °C it forms tetragonal (t), and at 2370 °C - cubic (c) fluorite structure [10]. The cubic lattice form can be stabilized at lower temperatures with the use of stabilizing agent, CaO, Y_2O_3 or other rare-earth oxides. The Y_2O_3 is one of the most common dopants, when tetravalent Zr^{4+} ion is exchanged for Y^{3+} ion which creates oxygen ion vacancy for every two yttrium ions to retain charge neutrality [11]. This process could be described using Kroger-Vink notation written in equation below:

$$Y_2O_3 \xrightarrow{ZrO_2} 2Y'_{Zr} + 3O_O^x + V_O^{\bullet\bullet}. \quad (1)$$

The equation (1) describes that Y'_{Zr} yttrium occupied lattice Zr position and dash shows that creates net negative charge, O is in its lattice site and there are no charge changes, $V_O^{\bullet\bullet}$ describes vacancy instead of oxygen with 2 positive net charges.

The crystal structure could be changed by varying yttria content in a sample as shown in **Fig. 1** [12]. The amount of yttria oxide required for full c stabilization is 8mol% and partial stabilization occurs at 2-5 mol% to form (t) [13]. The m phase remains stable only at low concentrations and low temperatures at elevated temperatures (above 1000 °C) YSZ undergoes martensitic transformation to a t phase, which causes a volume change of a unit cell by around 4%[12].

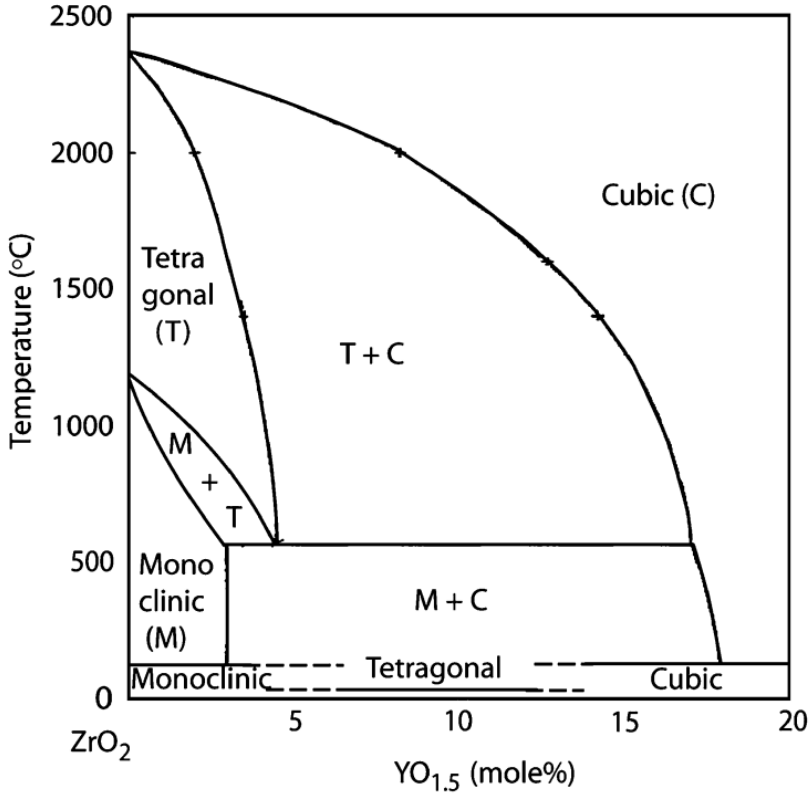

Fig. 1. Phase diagram of yttria-stabilized zirconia.[12]

As described in [14], the mechanism of dual phase formation is described as grain-boundary segregation-induced phase transformation (GBSIPT). Cubic phase starts to form from tetragonal phase from grain boundary region, where Y^{3+} ions tend to segregate, and this effect forces t-c dual phase formations inside a bulk region of a ceramic.

The density of sintered ceramics is affected by Y concentrations and sintering temperature. At lower sintering temperatures of 1100-1250 °C YSZ2 and YSZ3 samples exhibit higher relative densities than YSZ8. At temperatures of 1250 °C and larger YSZ8 samples relative density is higher[14][15]. This is explained by a sharp increase of average grain size which leads to better ionic conductivity. Grain sizes for YSZ2, YSZ3 and YSZ8 at lower than 1200 °C sintering temperatures grain sizes are similar about 0.2 µm, at higher temperatures grain sizes for YSZ8 samples increases faster than YSZ2 or YSZ3, at sintering temperatures of 1500 °C average grain size of YSZ8 is about 4 µm, YSZ2 and YSZ3 0.5 µm [14].

1.2 YSZ electrical conductivity

As previously mentioned, the addition of Y^{3+} instead of Zr^{4+} ion creates large amount of oxygen vacancies that are randomly distributed, which increases ionic transport of electrolyte[16], but ionic conductivity of YSZ ceramics is not proportional to dopant concentration as simple

transport theory suggested[10]. The highest conductivity is obtained using cubic zirconia with 8-10% added Y_2O_3 [7]. The long-range charge transport is affected by ceramics bulk resistivity, grain boundaries and is thermally activated, that could be described by Arrhenius equation[17]:

$$\sigma T = A\, exp\left(\frac{-\Delta E}{k_b T}\right), \quad (2)$$

Where σ is conductivity of a sample, A preexponential factor, ΔE activation energy, k_B Boltzmann constant.

Bulk conduction activation energies are characteristic of material, typical values are shown in **Table 1**, while conduction activation energies of a grain boundaries depends on ceramic manufacturing process[17]. Higher conduction activation energy value is observed at lower temperatures, low temperature activation energy values correspond to dopant concentration levels[18]. The lower activation energy of YSZ3 could result in higher bulk conductivity at lower temperatures, this is explained by lower concentrations of irregularities, dopants, vacancies for YSZ3 reducing dispersion of relaxation times [19]. High ionic conductivity of YSZ at higher temperatures are due to high mobility oxygen vacancies. Conductivity at 1000-1200K rises rapidly due to vacancy cluster breaking, that is predominant factor of conductivity at lower temperatures[15].

Table 1. Activation energy of crystal bulk ΔE_b, and standard deviation.

Material	ΔE_b, eV	Standard deviation	Reference
YSZ8 single crystal	1.05	0.05	[20]
YSZ8	1.09	0.07	
YSZ8 SPS	0.96	-	[7]
YSZ3	0.85	-	[21]
YSZ3	0.82	-	[19]
YSZ3	0.94	0.01	[22]

Grain boundary conductivity is typically lower by 3-4 times orders of magnitude compared to bulk conductivity [23]. The 2 main reasons for lower grain boundary conductivity are suggested. The first theory suggest that boundary conductivity is lower due to space charge layer formation around grain boundaries which have lower oxygen-vacancy concentration compared to grains bulk, this effect is seen when grain sizes are reduced and grain boundary conductivity rises due to reduced space charge potential, meanwhile slightly reducing bulk conductivity [23]. The second theory suggests that SiO_2 impurities forms siliceous films that lowers samples conductivity and reduces average grain size [24]. It is shown that small amounts

of SiO_2 for samples sintered at lower temperatures than 1200 K increases its conductivity, while sintered at higher temperatures conductivity decreases relative to pure YSZ samples, due to reduced sizes of grains compared to pure YSZ sintered at similar temperatures [22].

Spark plasma sintered or flash sintered YSZ8 samples have shown higher conductivity up to 50%[25] higher compared to conventional method prepared samples, primarily due to increased grain boundary conductivity. It is observed that increases in current density during flash sintering increases ionic conductivity of YSZ8[7], repeated sintering cycles increases conductivity to some limit [25]. Applied DC voltage induces electrochemical blackening. Partial reduction propagates from cathode to anode, which induces internal temperature gradient resulting in polarity dependent grain size and densification [26].

2. Experimental setup

2.1 Synthesizing YSZ pellets

Commercially available YSZ3 (ZrO_2 with 3mol% Y_2O_3), YSZ8 (ZrO_2 with 8mol% Y_2O_3 and surface area 12.4 m^2/g) and YSZ8n (ZrO_2 with 8mol% Y_2O_3 and surface area 129 m^2/g) powders were obtained. From each powder 2 samples were prepared by pressing them into green pellets. Green pellets are then sintered in a furnace, one of each powder sample was sintered at 1300°C and one of each at 1500°C respectively.

The YSZ8 SPS sample was obtained using spark plasma sintering (SPS) method. During this procedure the powder sample is simultaneously pressurized and sintered using high voltage pulsed electrical field, which leads to sintering temperature of 1100°C.

2.2 Density measurements

For measuring the density of YSZ pellets 2 techniques are used. The first technique is used when pellets are cylindrical shape, then diameter, height and mass of pellets are measured. Then density is calculated according to formula:

$$\rho(YSZ) = \frac{4m}{d^2 h\pi}, \tag{3}$$

where ρ is density, m is mass of a pellet, d is diameter, h height of pellet.

The second technique is used when pellets are not perfect cylindrical shape, and it is called Archimedes method for density measurements. Mass of the pellet is measured in air, and mass is measured when pellets is submerged in liquid. In this experiment acetone was used.

Experimental setup for measurement in acetone is shown in **Fig. 2**. Then equation below is used to calculate density of the pellet:

$$\rho(YSZ) = \frac{\rho(ace)*m(air)}{m(air)-m(YSZa)}, \quad (4)$$

where $\rho(ace)$ is density of acetone at environment temperature, $m(air)$ is mass of a pellet measured in air, $m(YSZa)$ is mass of a pellet measured in acetone.

Fig. 2. Setup for measuring mass of pellets in acetone. Bottom stand is used to hold vial with acetone, top stand is used to keep pellet submerged in acetone and not to touch the vial. Top stand stands on scales and is compensated.

2.3 Sample preparation

Preparations for impedance spectroscopy consists of filing samples down to about 2.5 mm diameter and height up to 1.5 mm, by hand using diamond files. Some of the samples are shown in **Fig. 3**. Sample of YSZ3 sintered at 1500 °C (YSZ3(15)) was formed with diameter d = 2.4 mm, surface area A = 4.523 mm^2, and height h = 1 mm. For YSZ3 sintered at 1300K (YSZ3(13)) sample rectangular shape is formed with 2 sides that we call height h = 1.6 mm apart, and electrode size of a = 4.4 mm, b = 0.5 mm, and an area A = 2.2 mm^2. The platinum paste is used to cover electrode surfaces, for YSZ3(15) sample of cylindrical shape that is flat surfaces, for YSZ3(13) surfaces that are 1.6mm apart. Covered samples are put in the furnace and is heated

up to 400K and is kept at this temperature for an hour to evaporate organic compounds that are used in platinum paste, after temperature is risen to 800K for platinum molecules to bind with surface of samples and form an electrode. After this sample is left to cool in a furnace slowly to avoid any defects due to thermal stress and temperature gradient.

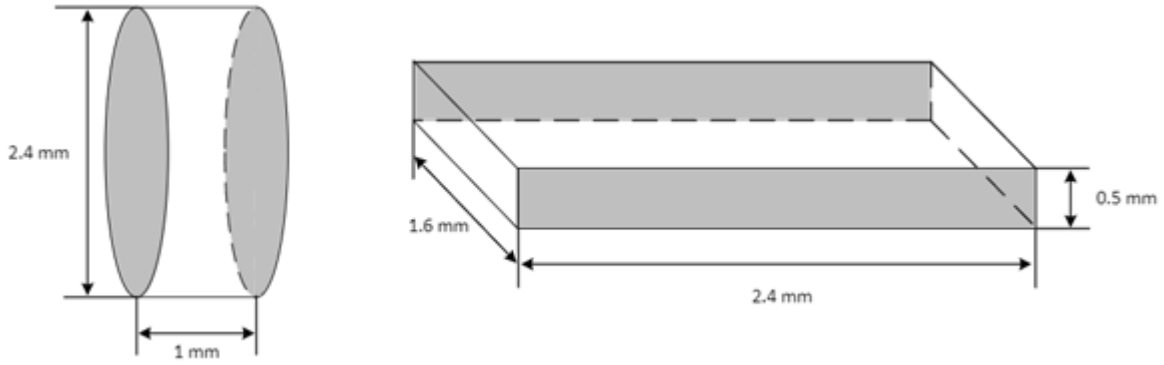

Fig. 3. Shapes and sizes of prepared pellets. Gray surfaces are covered with Pt paste. Left is YSZ3(15), right YSZ3(13) samples.

2.4 Impedance spectroscopy

Impedance spectroscopy is a powerful technique used to study ionic and mixed-ionic electronic conductors, and dielectric properties of materials across a wide range of frequencies. This method is used to measure complex impedance of a system, which describes the relationship between voltage and current in AC circuits. Complex impedance consists of a real part (resistance) and imaginary component (reactance). Measurement is done by applying AC signal to sample and measuring resulting current over frequency range from 10 Hz to $2x10^6$ Hz.

In this experiment 2 electrode measurement method is used, the measurement equipment scheme is shown in **Fig. 4**[27]. The two channel computer oscilloscope TiePie Handyscope HS3 with built in function generator is used to create sinusoidal signal that is applied to the sample through a buffer, current flowing through is measured using I-V converter, which is connected to CH1 of oscilloscope, the applied voltage is measured at buffer output and is connected to CH2 through switch S. The differential amplifier is used if 4 electrode method is used to measure voltage drop directly inside the sample.

Measurements are done in the temperature range between 300-800K, for heating custom computer-controlled heater is used, for accurate temperature measurements TMD90A digital thermometer is used, control logic, data acquisition and analysis are done using MATLAB software.

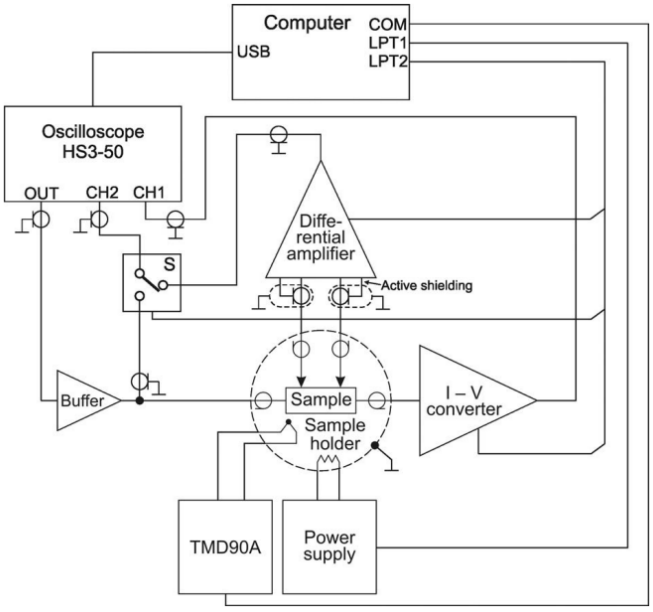

Fig. 4. Schematic overview of impedance spectrometer [27].

For complex impedance measurements geometrical factors must be considered. To eliminate differences of obtained results due to different sizes of samples equation:

$$Z^* = \frac{V}{I} = \rho \cdot \frac{L}{A}, \tag{5}$$

where Z^* is complex impedance, V describes applied voltage, I current flowing through a sample, ρ is resistivity of a sample, L distance between electrodes, A area of an electrode.

The impedance spectra are obtained in frequency range between 10 Hz - 2 MHz, for temperature from 300K to 800K with steps of 20K. Measurements are made while the temperature is increasing and decreasing.

3. Results

3.1 YSZ structure

`X-ray diffraction (XRD) measurements were obtained for 4 samples YSZ8(15), YSZ8n(15), YSZ SPS, YSZ3(15), according to [28], [29], measured peaks for YSZ8(15), YSZ8n(15), YSZ SPS correspond to cubic phase shown with o, and the peaks for YSZ3 marked by * correspond to tetragonal phase. Some smaller peaks appear due to reflections from sintered pellets, for more accurate results powder form should be used.

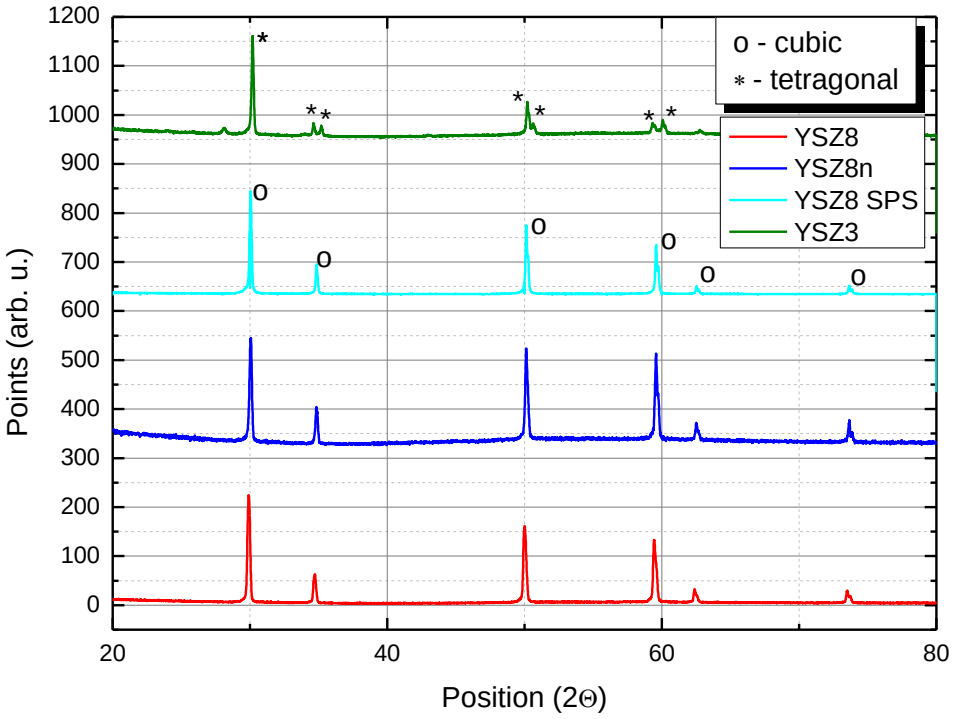

Fig. 5. XRD data of YSZ samples. o corresponds to peaks of cubic YSZ phase, * corresponds to peaks of tetragonal YSZ phase.

For samples sintered at 1500 °C and YSZ SPS SEM images were obtained in **Fig. *6*** with fixed magnification at 7000x. Some SEM images were obtained with a help of Le Mans University, shown in **Fig. 7**. YSZ8(15) has formed big and clearly distinct grains, with sizes about 4.55 µm. YSZ8n(15) grains are indistinct, clear lines are from polishing of sample surface, better results are shown in **Fig. 7**, where grain sizes are seen of sizes about 4.66 µm. YSZ SPS has formed typical YSZ8 grains, clusters of smaller particles in between grains are remains of removed material from polishing the surfaces, due to lower heating temperatures grain boundaries are not as distinct and accurate approximation of grain sizes are impossible. YSZ3(15) sample formed typical structure of small grains of sizes 0.63 µm.

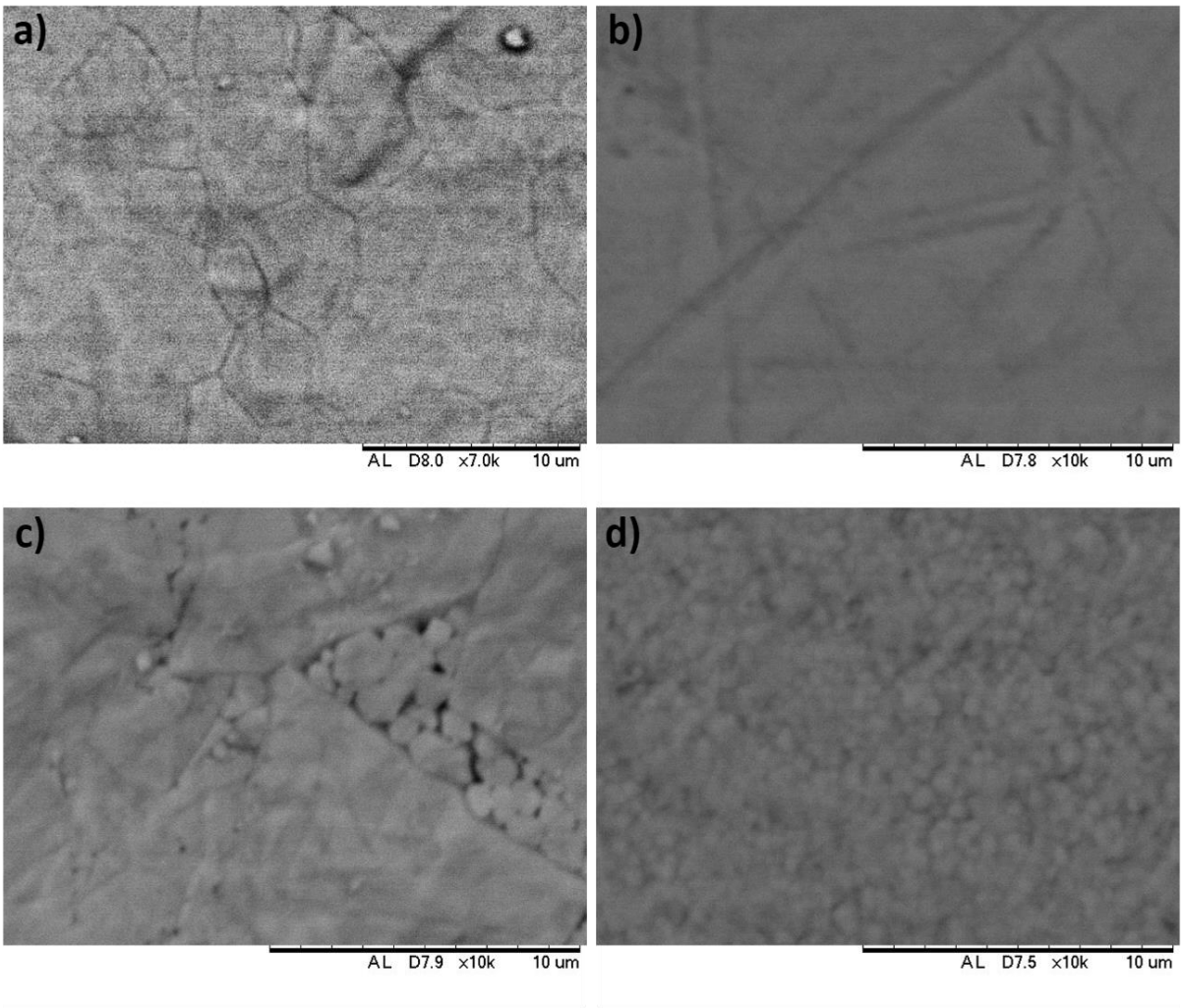

Fig. 6. SEM images of samples, a) YSZ8(15), b) YSZ8n(15), c) YSZ8 SPS, d) YSZ3(15), image magnification 7000x.

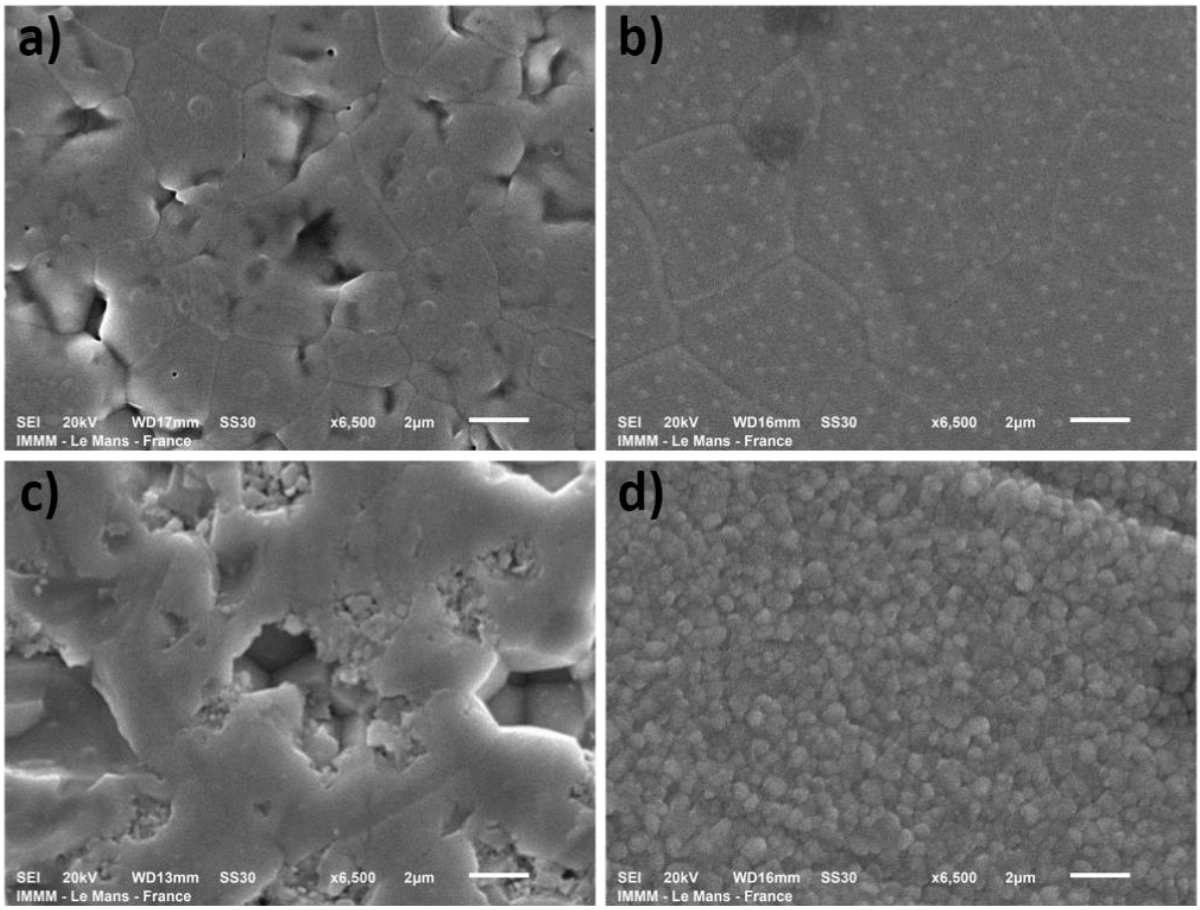

Fig. 7. SEM images of samples, a) YSZ8(15), b) YSZ8n(15), c) YSZ8 SPS, d) YSZ3(15), image magnification 6500x. Obtained with the help of Le Mans University.

3.2 Impedance spectra of YSZ ceramics

Impedance spectra of YSZ8(15), YSZ8n(15) and YSZ3(15) are presented in **Fig. 8**. In this graph 3 dispersion regions for each temperature are observed. At lowest temperatures this region corresponds to interactions between sample-electrode interface, in middle frequency range dispersion due to processes in grain boundary region could be observed, at highest frequencies dispersion appears due to processes in grains (bulk) of a sample. Arrows point to regions for each temperature corresponding to specified dispersion region.

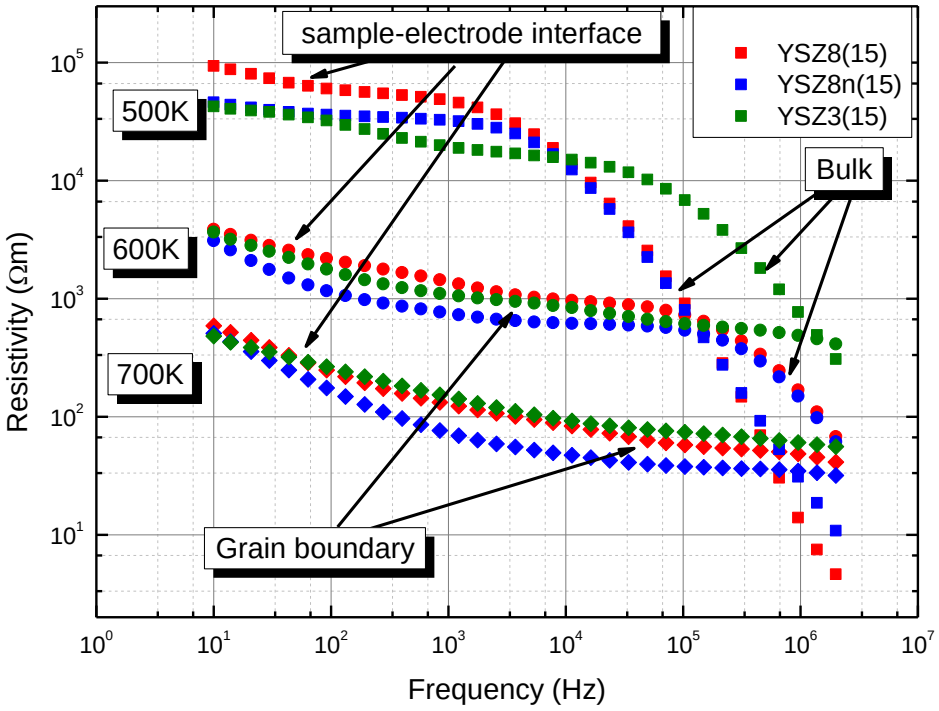

Fig. 8. The real part of impedance spectra for YSZ3(13), YSZ3(15) ceramics sintered at 1300 and 1500°C respectively.

For further impedance spectroscopy analysis complex impedance graphs are obtained **Fig. 9.** In these graphs the imaginary part dependency on real part is plotted. When the frequency of the applied voltage is varied, data are quite often distributed along parts of semi-circles, the chords of which, from low to large frequencies, allow to isolate the individual contributions of the bulk volume, grain boundaries and surface-electrode interaction. It could be observed that at temperatures slightly above room temperature YSZ samples are not conductive, while increasing temperature more of dispersion regions could be observed. For 400K only bulk region is observed at analyzed frequencies, at 500K grain boundary region appears, at higher temperatures electrode-surface region appears and at even higher temperatures dominates analyzed frequency range. For all three-dispersion analysis at higher temperature, higher frequency measurements must be done.

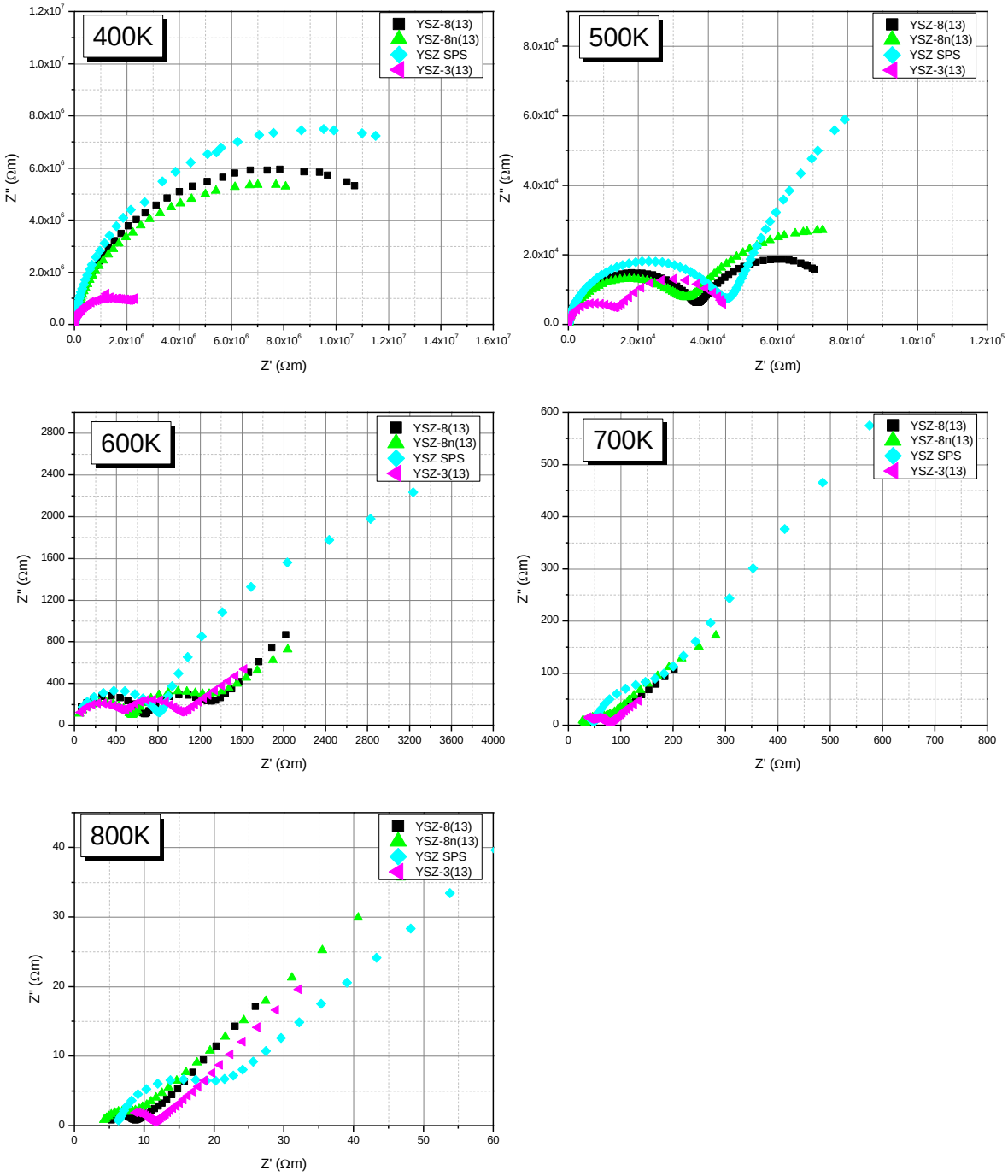

Fig. 9. Complex impedance plane plots for YSZ8(15), YSZ8n(15) and YSZ3(15) at temperatures of 400K, 500K, 600K, 700K and 800K.

3.3 Impedance spectra analysis

A basic procedure to analyze complex impedance graphs is to fit experimental data to equivalent circuit. In this work the equivalent circuit used is shown in **Fig. 10**. Complex impedance graphs have 3 distinct regions corresponding to processes happening in the ceramics' grains (bulk), grain boundaries, and sample-electrode interface from left to right on x axis respectively corresponding to lower frequencies **Fig. 11**. In the complex plane semi-circle curve could be described as RC circuit, real axis (Z') corresponds to resistance (R) component of RC circuit and could be estimated from distance between beginning of a curve to starting of forming of another semi-circle at a local minimum. The real value should be found where horizontal distance describes semi-circle diameter. The curve appears due to changes of imaginary axis (Z"), impedance that arises from capacitance features of a sample. For perfect RC circuits a perfect semi-circular curve should be observed, in this case curves are not perfect semi-circles, and capacitor in equivalent circuit is exchanged for constant phase element (CPE).

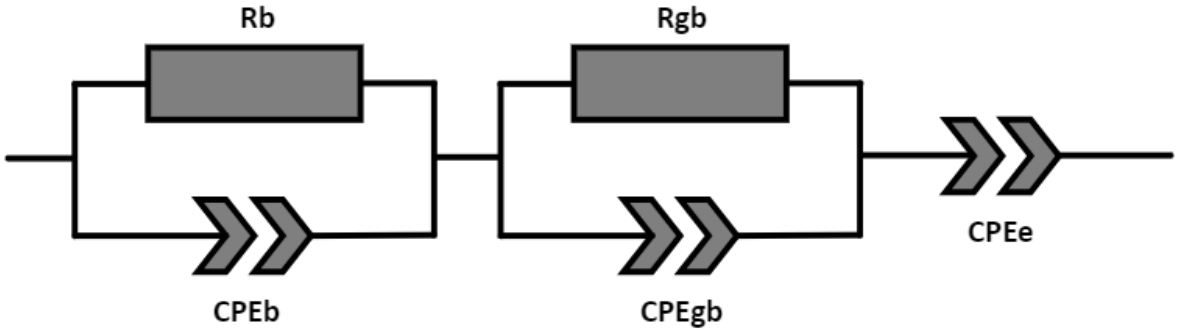

Fig. 10. An equivalent circuit is used to simulate and approximate the impedance of a polycrystalline material which is ionically conductive. Rb, CPEb denote resistance and capacitance of crystal bulk, and Rgb CPEgb denote the resistive and capacitive contributions of the grain boundaries, CPEe describes sample-electrode interface.

The CPE describes imperfect capacitor and its electrical impedance is:

$$Z_{CPE} = \frac{1}{Q(j\omega)^n}, \tag{2}$$

where $Q = 1/|Z|$, n could be from 0 to 1 and describes non ideality of CPE element when $n = 1$, CPE is perfect capacitor C, and $n = 0$, CPE is simple resistor R=1/Q. j is imaginary unit, ω – angular frequency measured in [rad/s].

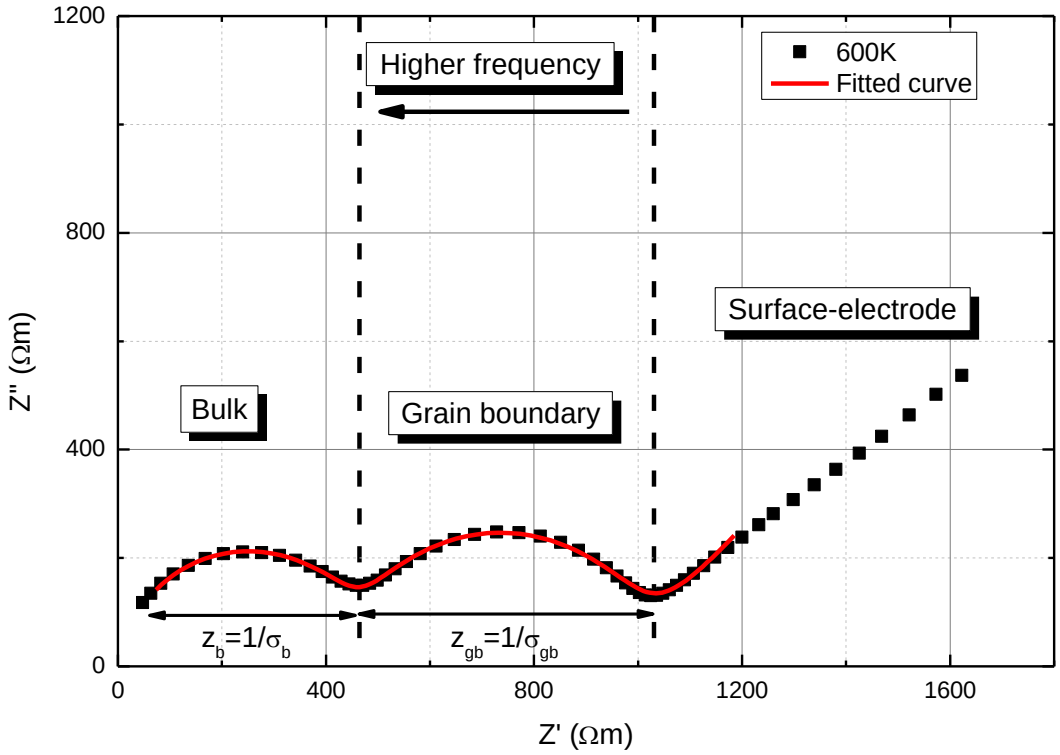

Fig. 11. Complex impedance plane analysis, with fitted curve of YSZ3(13) sample at 600K temperature.

To obtain accurate impedance values "ZView2" software was used to obtain fitted curves. For the accurate fitting approximate values were provided, and data points at the edges of measurement frequencies were ignored, for low frequencies which correspond to surface-electrode interactions, higher frequencies were avoided due to equivalent circuit not being a perfect representation of measured results and to increase accuracy in interested region. With equivalent circuit shown in **Fig. 10** fitted curve was obtained shown in **Fig. 11**. Values of fitted curve are shown in a **Table 2** below.

Table 2. Equivalent circuit data for fitting YSZ3(13) at 600K. Values corresponding to the first 3 elements describe the first semi-circle curve describing polycrystalline bulk, 4-6 describes grain boundaries, last two elements describe surface-electrode interface.

Element	**Value**	**Error**	**Error%**
R_b	532.50 Ωm	4.39 Ωm	0.83
CPE_b Q	0.164 µF/m	5.21 nF/m	3.19
CPE_b n	0.88	0.0034	0.39
R_{gb}	458.70 Ωm	0.93 Ωm	0.20
CPE_{gb} Q	3.42 nF/m	61.8 pF/m	1.81
CPE_{gb} n	0.90	0.001	0.13
CPE_e Q	87.68 µF/m	6.84 µF/m	7.80
CPE_e n	0.59	0.01	2.23

3.4 Temperature dependencies of YSZ conductivity

Acquired resistivity values were inverted to obtain conductivity, results shown in **Fig. 12** and **Fig. 13**. According to the Arrhenius equation (2) a linear fit corresponds to activation energies which were obtained and shown in **Table 3**. It could be observed that samples bulk conductivities are not affected by sintering temperatures or sample preparation methods, all YSZ8 samples follow a similar curve, and both YSZ3 samples are more conductive at low temperatures, at 600K conductivities are very similar for YSZ8 and YSZ3 materials, at higher temperatures YSZ8 samples exhibit higher conductivity. According to [19] this could be explained because of lower concentrations of irregularities, dopants, vacancies for YSZ3 reducing dispersion of relaxation times. Activation energies for YSZ8(13),YSZ8n(15) and YSZ SPS are ΔE_b = 1.035 eV, for YSZ8(15) and YSZ8n(13) ΔE_b = 1.050 eV, according to [17] YSZ8 activation energy could vary in the region ΔE_b = 1.036 ± 0.062 eV. Activation energies for YSZ3(13) and YSZ3(15) ΔE_b = 0.871 eV.

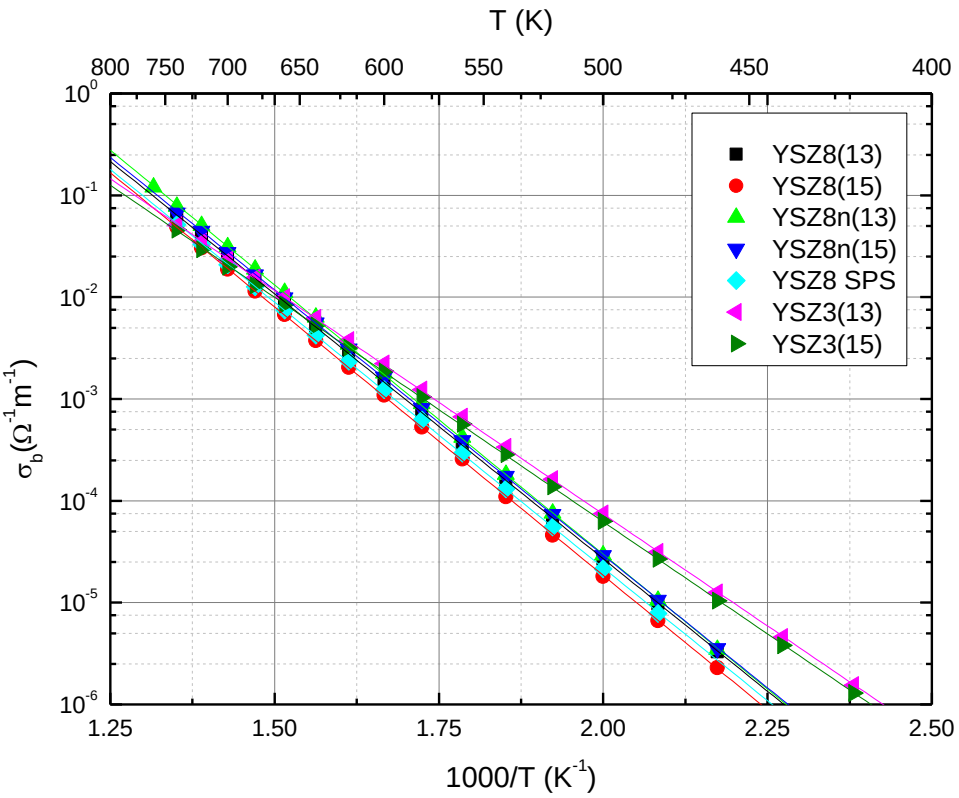

Fig. 12. Bulk conductivity dependency on inversed temperature. Slopes of curves describe activation energies for each sample (apparent linear fit).

It could be observed that grain boundary conductivities for all samples are about 2-3x lower compared to bulk conductivities. YSZ SPS has about 10 times lower conductivity compared to traditional method made samples, which could be due to sample being too porous for oxygen to transfer its energy from bulk crystallite to another. The effect of grain sizes could be seen for YSZ8(15) and YSZ8n(15) samples, bigger grain size of YSZ8n(15) compared to YSZ8(15), corresponds to higher grain boundary conductivity and lower conductivity activation energy, because of YSZ8n(15) being less porous and having smaller space charge region around grain boundaries. Activation energies for YSZ8(13), YSZ8(15), YSZ8n(13) and YSZ8 SPS are ΔE_b = 1.1 eV, for YSZ8n(15), YSZ3(13) and YSZ3(15) activation energies are ΔE_b = 1.045 eV.

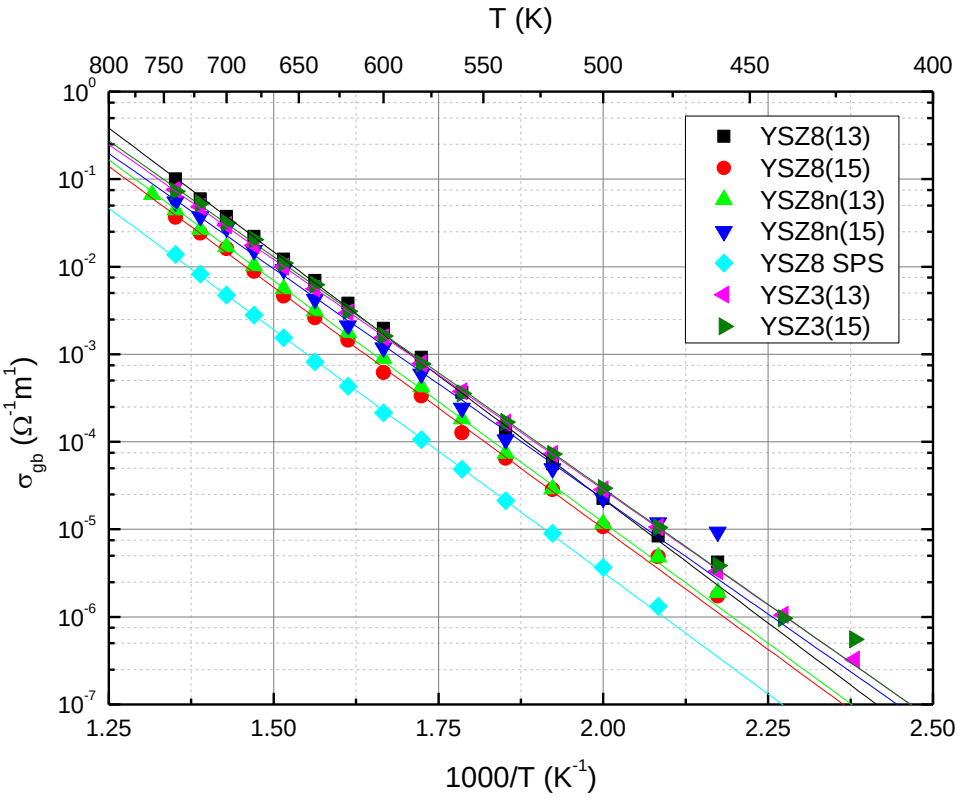

Fig. 13. Grain boundary conductivity dependency on inversed temperature. Slopes of curves describe activation energies for each sample (apparent linear fit).

Table 3. Obtained samples' activation energies of bulk and grain boundary conductivities, conductivities of bulk and grain boundaries at 500K respectively, density of samples.

Material	ΔE_b, eV	ΔE_{gb}, eV	σ_b at 500K, S/m	σ_{gb} at 500K, S/m	ρ, g/ml
YSZ8(13)	1.033 ± 0.002	1.122 ± 0.014	2.66 x10^{-5}	2.24 x10^{-5}	5.7
YSZ8(15)	1.048 ± 0.005	1.095 ± 0.032	1.83 x10^{-5}	1.06 x10^{-5}	5.87
YSZ8n(13)	1.051 ± 0.004	1.095 ± 0.016	2.96 x10^{-5}	1.16 x10^{-5}	5.89
YSZ8n(15)	1.035 ± 0.002	1.044 ± 0.033	2.91 x10^{-5}	2.27 x10^{-5}	5.64
YSZ8 SPS	1.037 ± 0.001	1.101 ± 0.014	2.19 x10^{-5}	3.67 x10^{-6}	5.94
YSZ3(13)	0.870 ± 0.003	1.043 ± 0.014	7.74 x10^{-5}	2.84 x10^{-5}	5.94
YSZ3(15)	0.872 ± 0.004	1.050 ± 0.023	6.21 x10^{-5}	2.95 x10^{-5}	6.14

4. Conclusions

YSZ ceramics were analyzed with impedance spectroscopy method over 300-800K temperature range. Obtained results:

- The electrical conductivity of YSZ samples bulk is only affected by yttria content, for temperatures lower than 600K YSZ3 samples exhibits higher conductivity, at higher temperatures YSZ8 samples exhibits higher conductivity. For grain boundary, the largest effect on samples conductivity has sintering method, for all samples sintered at traditional method conductivities were similar at 500K $\sigma_{gb\ avg}$ = 2.314 x10^{-5} S/m, while YSZ SPS σ_{gb} = 3.67 x10^{-6} S/m. Grain size effect on grain boundary conductivity is also observed, YSZ8n(15) having higher average grain size compared to YSZ8(15), results in higher grain boundary conductivity, for YSZ8n σ_{gb}= 2.27 x10^{-5} S/m at 500K, YSZ8 σ_{gb}=1.06 x10^{-5} S/m at 500K.
- The activation energy of ceramics bulk does not depend on sintering temperature, density, sintering method. The YSZ8 ceramics' bulk conductivity activation energy varies in the range of ΔE_b = 1.033 – 1.051, which is typical according to theory, YSZ3 ceramics exhibit lower conductivity activation energy, i.e. ΔE_b = 0.871 eV. The grain boundary conductivity activation energies of YSZ8 ceramics varies ΔE_b = 1.044 – 1.122, while YSZ3 activation energies are ΔE_b = 1.045 eV.

References

[1] B. Butz, "Yttria-Doped Zirconia as Solid Electrolyte for Fuel-Cell Applications," Karlsruher Institutes f¨ur Technologie (KIT), 2009. doi: 10.5445/IR/1000015724.

[2] Yang Gao, Mingming Zhang, Min Fu, Wenjing Hu, Hua Tong, Zetian Tao, A comprehensive review of recent progresses in cathode materials for Proton-conducting SOFCs, Energy Reviews, Volume 2, Issue 3, 2023, https://doi.org/10.1016/j.enrev.2023.100038.

[3] J. W. Fergus, "A review of electrolyte and electrode materials for high temperature electrochemical CO2 and SO2 gas sensors," *Sensors Actuators, B Chem.*, vol. 134, no. 2, pp. 1034–1041, 2008, doi: 10.1016/j.snb.2008.07.005.

[4] A. Q. Pham and R. S. Glass, "Oxygen pumping characteristics of yttria-stabilized-zirconia," *Electrochim. Acta*, vol. 43, no. 18, pp. 2699–2708, 1998, doi: 10.1016/S0013-4686(97)10179-7.

[5] M. Keane, M. K. Mahapatra, A. Verma, and P. Singh, "LSM-YSZ interactions and anode delamination in solid oxide electrolysis cells," *Int. J. Hydrogen Energy*, vol. 37, no. 22, pp. 16776–16785, 2012, doi: 10.1016/j.ijhydene.2012.08.104.

[6] Chen, M., Liu, Y.-L., Bentzen, J. J., Zhang, W., Sun, X., Hauch, A., … Hendriksen, "Microstructural Degradation of Ni/YSZ Electrodes in Solid Oxide Electrolysis Cells under High Current," *J. Electrochem. Soc.*, vol. 160, no. 8, pp. F883–F891, 2013, doi: 10.1149/2.098308jes.

[7] X. Vendrell, D. Yadav, R. Raj, and A. R. West, "Influence of flash sintering on the ionic conductivity of 8 mol% yttria stabilized zirconia," *J. Eur. Ceram. Soc.*, vol. 39, no. 4, pp. 1352–1358, 2019, doi: 10.1016/j.jeurceramsoc.2018.12.048.

[8] Y. D. Mundra R, Mishra TP, Bram M, Guillon O, "Sintering behavior of 8YSZ-Ni cermet: Comparison between conventional, FST/SPS, and flash sintering," *Int J Appl Ceram Technol.*, vol. 20, pp. 2271–2280, 2023.

[9] J. Langer, M. J. Hoffmann, and O. Guillon, "Electric field-assisted sintering in comparison with the hot pressing of yttria-stabilized zirconia," *J. Am. Ceram. Soc.*, vol. 94, no. 1, pp. 24–31, 2011, doi: 10.1111/j.1551-2916.2010.04016.x.

[10] J. F. Abelard, P. and Baumard, "Study of the dc and ac electrical properties of an yttria-stabilized zirconia single crystal," *Phys. Rev. B*, vol. 26, no. 2, pp. 1005–1017, 1982.

[11] J. R. Kelly and I. Denry, "Stabilized zirconia as a structural ceramic: An overview," *Dent. Mater.*, vol. 24, no. 3, pp. 289–298, 2008, doi: 10.1016/j.dental.2007.05.005.

[12] G. Witz, V. Shklover, W. Steurer, S. Bachegowda, and H. P. Bossmann, "Phase evolution in yttria-stabilized zirconia thermal barrier coatings studied by rietveld refinement of X-ray powder diffraction patterns," *J. Am. Ceram. Soc.*, vol. 90, no. 9, pp. 2935–2940, Sep. 2007, doi: 10.1111/j.1551-2916.2007.01785.x.

[13] S. Fabris, A. T. Paxton, and M. W. Finnis, "A stabilization mechanism of zirconia based on oxygen vacancies only," *Acta Mater.*, vol. 50, no. 20, pp. 5171–5178, 2002, doi: 10.1016/S1359-6454(02)00385-3.

[14] K. Matsui, H. Yoshida, and Y. Ikuhara, "Grain-boundary structure and microstructure development mechanism in 2-8 mol% yttria-stabilized zirconia polycrystals," *Acta Mater.*, vol. 56, no. 6, pp. 1315–1325, 2008, doi: 10.1016/j.actamat.2007.11.026.

[15] J. P. Goff, W. Hayes, S. Hull, M. T. Hutchings, and K. N. Clausen, "Defect structure of yttria-stabilized zirconia and its influence on the ionic conductivity at elevated temperatures."

[16] O. J. Durá, M. A. López de la Torre, L. Vázquez, J. Chaboy, R. Boada, A. Rivera-

Calzada, J. Santamaria, and C. Leon, “Ionic conductivity of nanocrystalline yttria-stabilized zirconia: Grain boundary and size effects,” *Phys. Rev. B - Condens. Matter Mater. Phys.*, vol. 81, no. 18, pp. 1–9, 2010, doi: 10.1103/PhysRevB.81.184301.

[17] P. Abelard and J. F. Baumard, “The electrical conductivity of cubic stabilized zirconia The Results of an IUPAC Collaborative Study,” W.-L. Ng, 1995.

[18] J. B. Goodenough, “Oxide-ion electrolytes,” *Annu. Rev. Mater. Res.*, vol. 33, pp. 91–128, 2003, doi: 10.1146/annurev.matsci.33.022802.091651.

[19] S. Kazlauskas, A. Kežionis, T. Šalkus, and A. F. Orliukas, “Charge carrier relaxation in solid $V_O^{\bullet\bullet}$ conductors,” *Solid State Ionics*, vol. 262, pp. 593–596, 2014, doi: 10.1016/j.ssi.2013.10.035.

[20] N. H. Perry, T. C. Yeh, and T. O. Mason, “Temperature dependence of effective grain core/single crystal dielectric constants for acceptor-doped oxygen ion conductors,” *J. Am. Ceram. Soc.*, vol. 94, no. 2, pp. 508–515, Feb. 2011, doi: 10.1111/j.1551-2916.2010.04093.x.

[21] X. Guo and Z. Zhang, “Grain size dependent grain boundary defect structure: Case of doped zirconia,” *Acta Mater.*, vol. 51, no. 9, pp. 2539–2547, 2003, doi: 10.1016/S1359-6454(03)00052-1.

[22] E. Drożdż, J. Wyrwa, K. Schneider, and M. Rękas, “Electrical properties of silica-doped 3 mol% yttria-stabilized tetragonal zirconia,” *J. Mater. Sci.*, vol. 52, no. 2, pp. 674–685, 2017, doi: 10.1007/s10853-016-0361-2.

[23] J.-H. Lee, T. Mori, J.-G. Li, T. Ikegami, M. Komatsu, and H. Haneda, “Improvement of Grain-Boundary Conductivity of 8 mol % Yttria-Stabilized Zirconia by Precursor Scavenging of Siliceous Phase,” *J. Electrochem. Soc.*, vol. 147, no. 7, p. 2822, 2000, doi: 10.1149/1.1393612.

[24] T. S. Zhang, J. Ma, Y. Z. Chen, L. H. Luo, L. B. Kong, and S. H. Chan, “Different conduction behaviors of grain boundaries in SiO2-containing 8YSZ and CGO20 electrolytes,” *Solid State Ionics*, vol. 177, no. 13–14, pp. 1227–1235, 2006, doi: 10.1016/j.ssi.2006.05.006.

[25] X. J. Chen, K. A. Khor, S. H. Chan, and L. G. Yu, “Preparation yttria-stabilized zirconia electrolyte by spark-plasma sintering,” *Mater. Sci. Eng. A*, vol. 341, no. 1–2, pp. 43–48, 2003, doi: 10.1016/S0921-5093(02)00079-5.

[26] M. Biesuz *et al.*, “Flash spark plasma sintering of 3YSZ,” *J. Eur. Ceram. Soc.*, vol. 39, no. 5, pp. 1932–1937, 2019, doi: 10.1016/j.jeurceramsoc.2019.01.017.

[27] Kežionis, A., Butvilas, P., Šalkus, T., Kazlauskas, S., Petrulionis, D., Žukauskas, T., … Orliukas, A. F, “Four-electrode impedance spectrometer for investigation of solid ion conductors,” *Rev. Sci. Instrum.*, vol. 84, no. 1, Jan. 2013, doi: 10.1063/1.4774391.

[28] J. C. Ray, R. K. Pati, and P. Pramanik, “Chemical synthesis and structural characterization of nanocrystalline powders of pure zirconia and yttria stabilized zirconia (YSZ),” *J. Eur. Ceram. Soc.*, vol. 20, no. 9, pp. 1289–1295, 2000, doi: 10.1016/S0955-2219(99)00293-9.

[29] Vasanthavel, S., & Kannan, S. (2018). Structural investigations on the tetragonal to cubic phase transformations in zirconia induced by progressive yttrium additions. *Journal of Physics and Chemistry of Solids*, *112*, 100–105. https://doi.org/10.1016/j.jpcs.2017.09.010

Summary

Naglis Burdaitis

The Influence of YSZ Ceramics Processing Method on Their Electrical Properties

The aim of this work was to investigate the influence of sintering temperature, method, size of powder grains on electrical properties of YSZ ceramics using impedance spectroscopy. Electrical properties of YSZ8 (ZrO_2 with 8mol% Y_2O_3 and surface area 12.4 m^2/g), YSZ8n (ZrO_2 with 8mol% Y_2O_3 and surface area 129 m^2/g), YSZ3 (ZrO_2 with 3mol% Y_2O_3), one of each sample sintered at 1300 °C and 1500 °C respectively and YSZ SPS sample sintered by using spark plasma sintering, were obtained by impedance spectroscopy method and analyzed using equivalent circuit fitting over temperature range 300-800K. XRD analysis of samples was performed and grain size was analyzed using SEM. The bulk conductivity only depends on material used, for samples made from YSZ8 powders conductivity were lower for temperatures below 600K compared to samples prepared using YSZ3 powder, and higher above. Grain boundary conductivity was the best for YSZ3(13) (σ_{gb} = 2.84 x10^{-5} S/m at 500K), and the worst of YSZ SPS (σ_{gb} = 3.67 x10^{-6} S/m at 500K) over the temperature range of 300-800K. Activation energies of ceramics bulk conductivity for YSZ8 varies in the range of ΔE_b = 1.033 – 1.051, for YSZ3 ΔE_b = 0.871 eV, grain boundary conductivity activation energies of YSZ8 ceramics varies ΔE_b = 1.044 – 1.122, while YSZ3 activation energies are ΔE_b = 1.045 eV.

Santrauka

Naglis Burdaitis

YSZ keramikų gamybos metodo įtaka jų elektrinėms savybėms

Šio darbo tikslas – impedanso spektroskopijos metodu ištirti sukepinimo temperatūros, gaminimo būdo ir miltelių grūdelių dydžio įtaką YSZ keramikos elektrinėms savybėms. Pagaminti iš viso 7 bandiniai, 6 tradiciniu būdu iš miltelių YSZ8 (ZrO_2 su 8mol% Y_2O_3 ir paviršiaus plotas 12,4 m^2/g), YSZ8n (ZrO_2 su 8mol% Y_2O_3 ir paviršiaus plotas 129 m^2/g), YSZ3 (ZrO_2 su 3mol% Y_2O_3), iš kurių po vieną bandinį sukepinome 1300 °C ir po vieną bandinį 1500 °C temperatūroje, taip pat YSZ SPS mėginys, kurį sukepinome naudojant kibirkštinio plazmos sukepinimo būdą. Impedanso spektroskopijos metodu gauti duomenys, analizuoti naudojant lygiavertės grandinės schemą, 300–800 K temperatūros diapazone. Atlikta mėginių XRD analizė, o grūdelių dydis išanalizuotas naudojant SEM. Tūrinis laidumas

priklauso tik nuo naudojamos medžiagos, mėginių, pagamintų iš YSZ8 miltelių, laidumas buvo mažesnis esant žemesnei nei 600 K temperatūrai, palyginti su mėginiais, paruoštais naudojant YSZ3 miltelius, ir didesnis aukštesnėje temperatūroje. Grūdelių tarpkristalitinis laidumas buvo geriausias YSZ3(13) (σ_{gb} = 2,84 x10^{-5} S/m esant 500 K), o blogiausias YSZ SPS (σ_{gb} = 3,67 x10^{-6} S/m esant 500 K) 300–800 K temperatūrų diapazone. Keramikos tūrinio laidumo aktyvavimo energijos YSZ8 kinta ΔEb = 1,033 – 1,051 diapazone, YSZ3 ΔE_b = 0,871 eV, YSZ8 keramikos grūdelių tarpkristalitinio laidumo aktyvavimo energijos svyruoja ΔE_b = 1,044 – 1,122, o YSZ3 tarpkristalitinio laidumo aktyvavimo energijos yra ΔE_b = 1,045 eV.